Elsevier Editorial System(tm) for Atmospheric Research
Manuscript Draft

Manuscript Number: ATMOSRES-D-11-00264

Title: Satellite and Surface-based Remote Sensing of Southeast Asian Aerosols and their Radiative Effects

Article Type: 7SEAS, Reid

Section/Category: remote sensing

Keywords: Southeast Asia; aerosol radiative effects; remote sensing

Corresponding Author: Mr Nan Feng, M.D.

Corresponding Author's Institution: University of Alabama in Huntsville

First Author: Nan Feng, M.D.

Order of Authors: Nan Feng, M.D.; Sundar Christopher, Ph.D.

Abstract: Using one year (December 2006 - November 2007) of Moderate Resolution Imaging SpectroRadiometer (MODIS), Multiangle Imaging SpectroRadiometer (MISR) and Clouds and the Earth's Radiant Energy System (CERES) data sets from NASA's Terra satellite, we assess the spatial and temporal distributions of aerosol properties (Aerosol Optical Depth, Fine Mode Fraction, and Single Scattering albedo) in the Southeast Asian (SEA). We also provide a quantitative evaluation of regional cloud-free diurnally averaged shortwave aerosol radiative effects (SWARE) at the top of atmosphere (TOA) over both land and ocean. Our results indicate that the diurnally averaged shortwave and longwave radiative effects at the TOA over ocean and land are(-6.4±1.2 Wm-2) and ocean (-5.9±1.3 Wm-2), respectively. The 550 nm aerosol optical depths are 0.27±0.24 and 0.12±0.10 over land and ocean. The variations and transports of regional aerosols have been studied based on monsoon meteorology. Fine aerosol particles (< 0.6μm)) are dominate over continental area during the whole study period, which represents large fractions of biomass burning aerosols and anthropogenic pollutant aerosols.. Our results also indicate that the monthly averaged cloud cover fractions over this region are above 60% and sampling aerosols underneath these cloud layers are further needed in future field campaigns.

Cover Letter

Atmospheric Research

Satellite and surface-based remote sensing of Southeast Asian aerosols and their radiative effects

Dear Editor

Please find enclosed our paper titled 'Satellite and surface-based remote sensing of Southeast Asian aerosols and their radiative effects' by Feng and Christopher for the 7seas special issue in Atmospheric Research.

Southeast Asia (SEA) is one of the areas with high aerosol concentrations, as a result of recent rapid urbanization and population growth during the past century. Pollution like biomass burning and dust from SEA can be transported across the North Pacific basin, reaching North America and beyond. Our paper uses multiple satellite data sets to evaluate the spatial and temporal variations of aerosols, and also assess the role of aerosols on the top of atmosphere radiative forcing in this region. We believe these results are significant to the research community.

With best regards,

Nan Feng

Department of Atmospheric Science
University of Alabama in Huntsville
320 Sparkman DR
Huntsville, AL 35805

Highlights

> We evaluate the spatial and temporal variations of aerosols over Southeast Asia. > Large fractions of smoke and industrial aerosols over Southeast Asian continent. > Satellite retrieved aerosols are in good agreement with ground-based measurements. > Aerosols radiative effects are calculated by using satellite measurements alone.

Satellite and Surface-based Remote Sensing of Southeast Asian Aerosols and their Radiative Effects

Nan Feng and Sundar A. Christopher

Department of Atmospheric Sciences, UAHuntsville, Huntsville, AL, USA

Abstract

Using one year (December 2006 - November 2007) of Moderate Resolution Imaging SpectroRadiometer (MODIS), Multiangle Imaging SpectroRadiometer (MISR) and Clouds and the Earth's Radiant Energy System (CERES) data sets from NASA's Terra satellite, we assess the spatial and temporal distributions of aerosol properties (Aerosol Optical Depth, Fine Mode Fraction, and Single Scattering albedo) in the Southeast Asian (SEA). We also provide a quantitative evaluation of regional cloud-free diurnally averaged shortwave aerosol radiative effects (SWARE) at the top of atmosphere (TOA) over both land and ocean. Our results indicate that the diurnally averaged shortwave and longwave radiative effects at the TOA over ocean and land are (-6.4±1.2 Wm^{-2}) and (-5.9±1.3 Wm^{-2}) respectively. The 550 nm aerosol optical depths are 0.27±0.24 and 0.12±0.10 over land and ocean. The variations and transports of regional aerosols have been studied based on monsoon meteorology. Fine aerosol particles (< 0.6μm) are dominate over continental area during the whole study period, which represents large fractions of biomass burning aerosols and anthropogenic pollutant aerosols.. Our results also indicate that the monthly averaged cloud cover fractions over this region are above 60% and sampling aerosols underneath these cloud layers are further needed in future field campaigns.

1. Introduction

Southeast Asia (SEA, 10°S~25°N, 90°E~150°E) comprising Vietnam, Laos, Cambodia, Thailand, Myanmar, Malaysia, and Indonesia is one of the areas with high aerosol concentrations, as a result of recent rapid urbanization and population growth. Biomass burning has existed for thousands of years in this region, which is a large source of atmospheric aerosols (Streets et al., 2009). Anthropogenic and natural organic carbon from extensive biomass burning and forest fires are estimated to contribute 38.2% of aerosol emissions, while anthropogenic and natural sulfate mainly from industrial and volcanic emissions show contributions of 27.8% and 14.0%, respectively (Streets et al. 2009),. During the period from 1980 to 2006, this region shows two large peaks in the 550 nm Aerosol Optical Depth (AOD, τ) values of about 0.35, corresponding to the Mt.Pinatubo volcanic eruption in 1991 (McCormick et al., 1995) and the huge forest fires in Indonesia in 1997. The increase in aerosols potentially has significant impacts on regional climate and air quality (Matsui et al., 2009).

Aerosols can modify the energy balance of the atmosphere by altering radiation budget, cloud properties and precipitation. On the other hand, they can also reduce air quality causing adverse health effects and poor visibility. SEA is recognized as a unique and complicated ocean-atmosphere-land environment for studying both the climatic effects and air pollution due to aerosol particles. It has also been well documented that pollution and dust from this region can be transported across the North Pacific basin, reaching North America and beyond, which makes this region more important for global and regional climate change and air quality research (Liu et al., 2003; Liang et al., 2007).

Smoke from biomass burning is among the major type of aerosols in Southeast Asia, which has a wide range of impact on climate, visibility and human health due to the emission of particle

matters and other gaseous pollutants such as CO, SO_x, NO_x and volatile organic compounds (Crutzen and Andreae, 1990; Kaufman et al., 1993; Streets et al., 2003). Smoke aerosols effects over Southeast Asia are studied largely from ground measurements that provide high temporal resolutions of aerosol properties such as optical thickness, size distribution, and concentrations (Begum et al., 2006; Chi et al., 2010; Sundarambal et al., 2010). However, satellite remote sensing is a valuable tool for studying the optical properties, radiative effects and transportations of smoke aerosols over large spatial scales. Several studies have been conducted over Africa and South America where a high frequency of biomass burning activities are prevalent (e.g. Edward et al., 2003; Patadia et al., 2008; Xu et al., 2010).

Since the launch of the Terra and Aqua satellites, new state-of-art of satellite sensors such as the Moderate Resolution Imaging SpectroRadiometer (MODIS) and the Multi-Angle SpectroRadiometer (MISR) have offered excellent capabilities for retrieving aerosol particle properties such as AOD and particle sizes from regional to global scales (Remer et al., 2005; Kahn et al., 2005). The radiative effect of aerosol particles at the top of atmosphere (TOA) can be calculated using aerosol particle properties from these observations and coincident broadband flux from radiative transfer model (Procopio et al., 2004) or from data sets such as the Clouds an the Earth's radiance Energy System (CERES) (Christopher et al., 2006). These measurements are now being used to validate numerical models and are also being used in data assimilation to improve forecasts of smoke aerosol properties and their radiative impacts (Reid et al., 2009).

In this study we first study the annual and seasonal spatial distributions of the AOD in the region based on MODIS level 2 aerosol products. Then we evaluate the ground-based AOD for the Aerosol robotic network (AERONET) locations along with MODIS and MISR AODs for December 2006 to November 2007. The reason we chose the year 2007 is that more available

AERONET measurements covering the whole region can be collected comparing to other periods. Furthermore, temporal variations of aerosol properties are studied based on information available from satellite-based sensors. Finally, the spatial distributions of shortwave direct aerosol radiative effects over both land and ocean are derived from CERES. Satellite remote sensing can provide reliable information on aerosol at large spatial scales as described in this study, while field campaigns referring aircraft measurements coupled with ground and satellite data sets can provide significant contributions for validating models and for isolating the impacts of aerosol particles on weather and the environment. Our goal is to provide a satellite remote sensing framework for modeling and experimental communities to better understand the emissions, transports and radiative transfers of atmospheric aerosols, meteorology and climate interaction in this region.

2. Data and methods

We used Aerosol Robotic Network (AERONET) data 10°S~25°N, 90°E~150°E) along with the Terra–MODIS and MISR aerosol products from December 2006 to November 2007. AERONET is a ground-based remote sensing aerosol network that using sun-photometers to provide AOD at seven wavelengths and properties such as aerosol size, absorption/scattering characteristics, and precipitation information. These well calibrated measurements are available from several hundred worldwide locations (Holben et al., 1998). In this study, both MODIS and MISR AOD were evaluated using available AERONET dataset in the study period from 14 sites covering most studied area (Figure 1a). Note that it is not the goal of this study to provide comprehensive validation of the satellite product with AERONET. We simply perform an

92 intercomparison between satellite and AERONET to ensure the quality of the radiative forcing
93 results. .

94 Based on multi-spectral observations, MODIS has been used to identify aerosols and their
95 properties with a high degree of confidence (Remer et al, 2005). Terra MODIS provides high
96 resolution global retrievals of aerosol properties including AOD and Fine Mode Fraction (FMF)
97 that represent total and size based aerosol concentration. The Collection 5 AODs are available
98 over dark targets such as oceans and vegetated areas, and the uncertainty of MODIS AOD data
99 has been estimated to be $0.03 \pm 0.05\tau$ over ocean and $0.05 \pm 0.15\tau$ over land (Remer et al., 2005;
100 Levy et al., 2007). Other biases in the MODIS products have also been reported elsewhere
101 (Zhang and Reid, 2006; Hyer et al., 2011). Over-ocean, retrieval biases are mainly generated
102 from sources including lower boundary condition (e.g., wind speed, white-capping and glint),
103 cloud contamination, and aerosol microphysical properties (e.g. assumed size, absorption, and
104 dust nonsphericity). Over-land, the important sources of errors comprise various random errors
105 (e.g., atmospheric path length, scattering angle "hot spot") and systematic biases (e.g., snow and
106 cloud contamination, surface albedo bias). The precision of retrieved AOD over land is lower
107 than over the ocean, because the land surface is brighter, more heterogeneous, and with more
108 strong and complicated aerosol sources than the ocean surface. Given assumptions about the
109 shape of the aerosol size distribution, MODIS FMF product defined as the fraction of fine mode
110 aerosols can be an important parameter to identify different types of aerosols, although it is
111 reported to be biased high in some regions (e.g. dust-impacted area, Chu et al., 2005).

112 In this study, Terra MODIS level 1B radiances are used to show an example of reflected solar
113 radiation of clouds and aerosols in the study area, and we also describe the annual mean spatial
114 distribution of AODs based on the Terra MODIS level 2 aerosol product. Regional aerosol

115 transportations in different seasons are accessed by using Navy Operational Global Atmospheric
116 Prediction System (NOGAPS) winds at 850 hPa.

117 We also used MISR data to report 558 nm AOD and single scattering albedo (SSA). MISR on
118 Terra has 9 cameras that measures upwelling solar radiance in four spectral bands (centered at
119 446, 558, 672, 866 nm) at nine view angles in the forward and aft directions along the flight path
120 (nadir, ±70.5º, ±60º, ±45.6º, ±26.1º from nadir). The wide range of view angles makes it feasible
121 to evaluate surface contribution to the TOA radiance accurately and hence retrieve aerosol
122 properties both over ocean and land surfaces including bright desert regions which can be
123 contaminated by sunglint for a mono-directional instrument (Diner et al., 1998; Kahn et al.,
124 2005). SSA retrieved from MISR is a beta version product, which is mainly used as an
125 exploratory indicator to identify major aerosol types.

126 To assess the instantaneous top of atmosphere shortwave radiative fluxes between clear and
127 aerosol sky regions, we use broadband (0.2–4.5 μm) shortwave fluxes from the Clouds and the
128 Earth's Radiant Energy System (CERES) scanners on Terra. The well calibrated CERES
129 radiances are converted to fluxes using empirical Angular Dependence Models (ADMs). The
130 current CERES-SSF product does not contain empirical ADMs as a function of sun-satellite
131 viewing geometry, AOD, and aerosol size. Using the Tropical Rainfall Measuring Mission
132 (TRMM) data for the tropics and a radiative transfer model, these ADMs are constructed by
133 assuming that all aerosols are pure scatterers (Loeb et al, 2003). Using Terra data, Zhang et al.
134 (2005a) constructed a complete set of ADMs using MODIS AOD and particle size information
135 over the global oceans. The differences in TOA fluxes between the CERES-SSF ADMs and
136 those developed by Zhang et al. (2005a) are larger than $10 Wm^{-2}$ per unit AOD. In this study, the
137 clear sky fluxes are estimated over the oceans and lands respectively by regressing the AODs

versus the shortwave fluxes. The regression line representing the relationship between fluxes and AODs is fitted to pixel level data. The flux extrapolated to zero AOD is then identified as the clear sky flux (Christopher, 2011). The difference of fluxes between the CERES clear and aerosol pixels at the TOA is called the Direct Radiative Effect (DRE), which provides a quantitative assessment of how aerosols change the TOA shortwave fluxes (Christopher et al., 2006). Slopes estimated from the regression relationship between DRE values and AODs may be affected by outliers. To minimize these effects, median values are used to develop regressions. Since biomass-burning aerosols prominent in Southeast Asia are largely dominated by fine mode particles, their impact in the longwave is negligible (Kaufman et al., 2000). Hence, the shortwave instantaneous DRE is derived in this study, which was further converted to diurnally averaged DRE using techniques described in Kaufman et al (2005).

3. Results and discussions

3.1 Annual and seasonal spatial distributions of aerosols

Figure 1a shows an example of a biomass burning event that occurred over several Southeast Asia countries on Feb. 03, 2007. Using red (0.620μm), green (0.545μm), and blue (0.459 μm) channel radiances, highly reflective clouds can be seen in white, haze caused by smoke aerosols over land can be seen in grey, whereas the ocean background has a dark blue appearance (Fig.1a). This region has been largely dominated by forest/woodland and wetlands, while the total fractions of forest area are larger than 50% in several countries including Malaysia and Indonesia. However, due to increasing urbanization, deforestation, and agriculture, variations of land use and surface cover in Southeast Asia has dramatically risen since last century (Klein Goldwijk, 2001). It has been reported that this region has experienced approximately 0.42% annual forest

degradation and 0.71% annual net cover change during the 1990-1997 period, which are both ranked as the highest rates in the world during the same period (Achard et al., 2002). Large amount of smoke aerosols can be generated from biomass burning processes, which is one of the major land cover change processes in this region. In the northwestern part of this image (Fig. 1a), the smoke can be seen from Thailand to Myanmar, and appears thicker to the west, because those smoke from fires might be combined with industrial and urban air pollution from farther west (Begum et al., 2006). The smoke haze events that took place from Cambodia and Thailand to Myanmar during February 2007 were due to the occurrence of hundreds of bush and forest fires, burning off crop residue for agricultural activities, and for clearing old pasture in preparation for new spring growth.

Figure1b shows the annual spatial distribution of MODIS Collection 5 AODs from the operational algorithm, with color scale from blue to red corresponding with low to high AODs. These AODs are retrieved over cloud-free ocean and dark surface areas. In a latitudinal band from 8 to 25°N, high AOD can be seen over land and coastal area from Myanmar in the west, across Thailand and Vietnam to the Taiwan Island in the east. Biomass/coal burning from both natural and anthropogenic sources contributes significantly to these high loadings (Pochanart et al., 2003; Tang et al., 2003; Gadde et al., 2009; Chi et al., 2010). Just south of 8°N, high AODs values are also seen around megacities such as the Singapore (1.28°N, 103.83°E) and Jakarta (6.2°S, 106.8°E), over Indonesia, which are highly correlated with anthropogenic and urban activities. In those metropolitan areas, there are significant emissions from automobiles and other anthropogenic activities related to the extremely high population density. The annual spatial distributions of Terra-MODIS AOD in Fig.1b are highly correlated with distributions of annual CO emissions data from the EDGAR 3.2FT2000 database (Olivier et al., 2005). Unlike Europe

and North America, where anthropogenic emissions are largely from fossil fuel combustion, in Southeast Asia, emissions from biofuels and biomass burning play a key role in the regional photochemistry. Inefficient combustion of biofuels at low temperatures can result in large emissions of CO, which is one of the main components of aerosols in Southeast Asia. In contrast, these low temperatures prevent the formation of thermal NOx, leading to comparatively smaller NOx emissions in this area (Phadnis et al., 2002).

To assess the spatial distributions of aerosols in different seasons over the SEA region, seasonal mean Terra-MODIS AOD distributions are shown in Figure 2, along with the Navy Operational Global Atmospheric Prediction System (NOGAPS) 850hpa winds at 2.5° resolutions averaged for each season. The regional meteorology is dominated by the Asian monsoon circulation, which can effectively determine the outflow and long-distance transport of aerosols in this region (Lawrence and Lelieveld, 2010). During the winter time (Fig.2a), the dry phase of the northeast monsoon is underway, which transports smoke due to biomass burning over the ocean further westward into the Indian Ocean. In these winter months, high AOD values (> 0.5) can also be seen over the ocean near coastal regions, because wind directions are from the land to the ocean areas. In the summer time (Fig.2c), intense monsoon rains effectively remove aerosols from the atmosphere. As a result, AOD values in the whole region, especially in the latitudinal band from 10°S to 5°N, are generally lower compared to the dry season. However, under the effects of strong southwest monsoon during these summer months, a fraction of insoluble pollutants, mostly from biomass burning, can still be transported towards the northeast, across the North Pacific basin, further reaching North America and beyond, which has also been highlighted by some previous studies (Liu et al., 2003; Liang et al., 2007). Between the summer and winter monsoons are the Monsoon Transition Periods (MTPs), during which the meridional

winds weaken, and zonal trade winds become strong around the equator. These MTPs can be referred to as 'onset-MTP' and 'withdrawal-MTP', indicating before and after the summer monsoon respectively (Fig. 2b,d). For the onset-MTP, similar with winter monsoon, the mean wind directions are still found from Southeast Asia to the Bay of Bengal, but a little weak in wind speeds (7.2m/s) In contrast to winter months, high AOD values over 0.5 can be seen in large areas of coastal regions such as southeastern China and Vietnam during the onset-MTP (Fig2b). Under the rapid increase of aerosol loadings in this period, the average values of AOD of this region reach peak values. Based on several satellite retrieval data sets, previous studies have observed extremely strong influence of biomass burning in Indonesia on the eastern equatorial Indian Ocean in several MTPs, especially during El Nino years (Heil and Goldammer, 2001; Li and Ramanathan, 2002). On the other side, the winds in the withdrawal-MTP are notably different from those in onset-MTP, with weaker westerly and mainly towards the Pacific. The AOD values generally drop to low values for the whole year, while the rapid decrease in pollutant levels can be expected in most areas.

Terra MODIS cloud dataset was used to investigate cloud cover in Southeast Asia. Higher amounts of cloud can be observed over Southeast Asia (e.g. Philippines, Indonesia, and Malaysia) in relation to the mid-latitude jet stream instability. From June to November, the summer monsoon is prevalent over Southeast Asia, which is generally humid with high levels of clouds cover (monthly mean cloud cover fraction of 60%~70%), whereas from December to May, the winter monsoon is the dominant system, which is dry with low cloud cover (cloud cover fraction of 50%~60%). Abundant cloud cover for the region of interest is a big challenge for aerosol detection, which reducing the availability of satellite-derived data thereby causing a potential undersampling.

3.2 AERONET AOD compared with MODIS and MISR

In this section we compare MODIS and MISR level 2 AODs with AERONET values. We selected all 14 AERONET sites with available AOD data, and compared those surface-based data collocated in time (±15 minutes) and space (0.5°×0.5°) (Table 1). In general the yearly mean MODIS (0.52±0.359) and MISR (0.33±0.158) observed AOD are in agreement with the yearly mean values reported by AERONET, (0.43±0.300 and 0.42±0.257), respectively. MODIS has more coincident AOD values with AERONET than MISR, because of its orbital characteristics. The swath width of MISR allows for only four or five overpasses per month for any 17.6*17.6 km^2 region in the Southeast Asia, not all of which have AOD values due to, for example, cloud cover. It can be seen in Table 1 that, comparing to MISR AODs, MODIS AODs compare well with AERONET AODs around urban areas with dark background and far from the ocean, e.g. Taipei_CWB with MODIS (0.41±0.31) versus AERONET (0.40±0.27), and Mukdahan with MODIS (0.44±0.30) versus AERONET (0.46±0.34). By contrast, better performance by MISR than MODIS, relative to AERONET AOD, can be found in stations close to coastal regions, such as Bac Giang, Bac Lieu, and Singapore, because MISR with more viewing angles than MODIS can retrieve aerosol optical properties over complicated terrains, whereas stations close to the sea will contribute more systematic errors in the MODIS AOD retrievals (Chin et al., 2004; Abdou et al., 2005; Kahn et al., 2007).

All collocated points of satellite and surface-based observations are shown in figure3 with regression and density analysis results. In general, MODIS AODs show better correlations with AERONET AODs than MISR AODs with a slope (1.075) very close to 1.0, and a relatively smaller intercept of about 0.05. This result also indicates MODIS collections 005 AOD data are

253 calibrated with more accurate retrievals than previous versions of MODIS AODs. Remer et al.,
254 (2005) used two years of Terra Collections 003 and 004 AOD data from MODIS to validate
255 against the collocated AERONET AOD values over land thus including about 5906 data points
256 representing global data. Their validation effort showed a slope of 0.78 and the intercept of 0.068
257 at the same wavelength of present study. The density maps are plotted by counting the numbers
258 of pixels in the unit area (AOD value 0.1×0.1). Dense pixels regions are labeled in red and
259 yellow colors, which are apparently within allowed uncertainties and prominent in lower values
260 of AODs. According to density maps, MODIS AODs show a distinct positive bias at low optical
261 thickness values (0~0.4) due to inadequate characterization of surface reflectance in some cases
262 (Remer et al., 2005; Levy et al., 2005). By contrast, MISR compares well with AERONET
263 AODs at low optical thickness values, whereas the uncertainties are larger at high values (> 0.5).
264 Possible reasons for these uncertainties could be related to the algorithm assumptions and
265 calibration methods, which have been noted in previous studies (Abdou et al., 2005; Kahn et al.,
266 2007; Kahn et al., 2009). Besides, our study also shows that during summer and winter, MISR
267 AOD values are much closer to AERONET than MODIS, while both satellite retrievals are
268 shown relatively poor performance during spring time.
269
270 **3.3 Temporal variations of aerosol properties over oceans and lands**
271 To assess the aerosol properties in Southeast Asia from MODIS and MISR, we show the time
272 series plots of 550 nm daily averaged AODs, FMFs (from MODIS), and SSAs (from MISR) over
273 both land and ocean in Fig. 4 from December 2006 to November 2007. In order to smooth the
274 data, the data for each day are replaced by the three-day moving average value. As has been
275 mentioned above, the winter and spring seasons are dominated by biomass burning aerosols

originating from the Thailand and Indonesia and reaching the Indian Ocean. Fig. 4a and 4b show that the maxima of AOD values over both land and ocean appear during winter and spring. For MODIS retrievals (Fig. 4a), there are peaks shift in origin from land to ocean over the period of March to May, which can be caused by continuous winter-spring monsoons mainly from land to ocean. In summer months, averaged MODIS AOD decreases rapidly to low values of 0.165 over land and 0.117 over ocean, due to precipitation scavenging. Those peaks in winter-spring time and valleys in summer time can also be seen in MISR AOD (Fig 4b), although it shows evident underestimations of AOD during the whole period.

Fig.4c and d show the time series of MODIS FMF and MISR SSA over both land and ocean. According to related results from satellite data and aerosol transport models, biomass burning smoke aerosols and regional anthropogenic pollution have particle sizes (volume mean diameter) in a narrow range of 0.26-0.3 μm (Kaufman et al., 2002; Reid et al., 2005), which is defined as fine particles (< 0.6 μm) by the MODIS retrievals. In contrast, natural or mechanistically produced aerosols (e.g. dust and sea salts) that are widespread over ocean and continents have predominantly coarse particles (>0.6 μm) (Chin et al., 2002). The temporal variation of particle size characteristics can be estimated based on the FMF values from MODIS (Fig.4c), which can be used to separate natural from anthropogenic aerosols (Kaufman et al., 2002). It can be seen that fine particles (>70%) dominate over continental area during the whole study period, which represents large fractions of biomass burning aerosols and anthropogenic pollutant aerosols in this area. Over the ocean, the fractions of fine particles are low during most months, except for some spring months with higher transportations of fine aerosol particles from land. In fig. 4d, the time series of MISR SSAs were also evaluated over land and ocean. Since MISR SSA data are only beta validated, these data are used as qualitative indicators and our interpretations must be

used with caution. At 550 nm, MISR SSAs values during the selected period are following common trends over land and ocean, respectively, where SSA is relatively lower in spring than that in other seasons. Higher concentrations of relatively 'dark' aerosols with lower SSA values can be seen in seasonal transition months (e.g. February, March, and September), which indicates a rise of large fractions of biofuel or biomass burning smoke particles during winter-spring and summer-fall time. All available AERONENT SSAs data during the selected period are also used to qualitatively compare with MISR SSAs, which are derived from ground-based radiance measurements. Satellite retrieved SSAs are in reasonable agreement with ground-based values, though monthly averaged AERONET SSAs appear to be substantially lower than MISR SSAs. Strong absorption of the direct solar radiation with lower SSAs values (0.8-0.9) can also be observed in those transition months.

3.4 Shortwave aerosol direct radiative effect over oceans and lands

Multiple sensors onboard satellites can be effectively used for studying aerosol climatic impacts from an observational perspective (Christopher and Jones, 2008; Patadia et al., 2008; Patadia et al., 2010). It can be seen in Fig. 5 that there are evident linear relationships between the MODIS AODs and the CERES Shortwave Aerosol Radiative Effects (SWARE) over land and ocean with high linear correlation coefficients reach -0.976 and -0.996, respectively. Due to different aerosol properties and underlying surface information, the quantitative relationships between AODs and SWARE over land and ocean are also different (Fig.5). The standard deviations of SWARE over land are much larger than that over ocean, especially when the AOD values are higher than 0.5. Large uncertainties can be found in estimations of SWARE over land , that is discussed in detail in section 3.5.

322 The SWARE is the difference between top of atmosphere (TOA) shortwave flux over clear sky
323 and aerosol sky. These instantaneous values are usually obtained from satellite observations and
324 converted to diurnal averages for comparison purposes (Zhang et al., 2005b). Fig. 6 shows the
325 spatial distributions of the diurnally averaged SWARE over Southeast Asia, which are calculated
326 over land and ocean independently, but combined in the same figure. Previous studies have
327 shown that the SWARE values mainly vary as a function of regions (Yu et al., 2006, Patadia et
328 al., 2008). The regional patterns of AOD compares well with the SWARE patterns with both
329 large AOD and SWARE over the ocean close to coastal region of Thailand, Vietnam,
330 southeastern China, and Taiwan due to a combination of biomass burning smoke and pollution
331 aerosols (Kaufman et al, 2002). Over land, higher SWARE are due to anthropogenic pollutions
332 over megacities, e.g. Singapore. In contrast, large AODs in the Southern China, Thailand and
333 Eastern Indonesia do not result in strong SWARE values. It might be due to the combined effects
334 of aerosol and surface properties from diverse ecosystems (Patadia et al., 2008). For more
335 absorbing aerosols, the overall SWARE can change from a negative to a positive effect
336 according to their size and underlying surface (Fig. 5). However, annual averages over 1°×1°
337 grids in Fig. 6 are largely negative.
338 The annual mean SWARE information from Terra CERES SSF products are given in Table 2.
339 Annual averaged shortwave fluxes of clear and aerosol covered sky over land area are both much
340 higher than that over ocean, whereas their differences are used to calculate instantaneous
341 aerosols direct radiative effects. The diurnally averaged annual SWARE is -6.4 Wm^{-2} over land
342 area and -5.9 Wm^{-2} over ocean corresponding to a mean clear-sky total AOD (from CERES
343 footprint) of 0.27±0.24 and 0.12±0.10, respectively. In comparison, Yu et al., (2006) use MISR
344 AOD along with assumed aerosol properties in radiative transfer models and report aerosol

radiative effects in different regions, where the SWARE values over Southeast Asian (0°N~30°N and 90°E~180°E) is about -7.2 Wm^{-2} over land with a mean AOD value of 0.31 and -4.5 Wm^{-2} over ocean with a mean AOD value of 0.13. The difference between satellite-model integrated estimation (Yu et al., 2006) and present study could be associated with heterogeneous aerosol loadings and the different selected area in present study (10°S~25°N and 90°E~150°E). Overall differences are likely due to the use of different datasets and cloud screening techniques. Yu et al. (2006) used MISR level 3 1°×1° MISR AOD values for land and MODIS level 3 1°×1° MODIS AOD values for ocean while we use level 2 MODIS AOD collocated in CERES SSF products. Also, we use stringent cloud screening criteria to ensure that the CERES data are not contaminated with clouds while requiring 99% of the CERES footprint to be cloud free. Besides, sample biases due to different spatial resolutions between MODIS (10×10 km^2) and CERES footprint (20×20 km^2) are estimated to globally reduce SWRE by an average of 30% (Christopher and Jones, 2008). We have multiplied mean MODIS AOD minus the CERES AOD by a radiative efficiency value to correct the clear sky sample biases. Shortwave radiative efficiency (Wm^{-2} per unit AOD) is the efficiency of aerosols in perturbing the shortwave radiation at the top of atmosphere, which is a key parameter for studying the climatic effects of aerosols. Zhang et al. (2005b) reported that the aerosol radiative efficiency is sensitive to the fine mode fraction, while higher fine mode fraction can result in lower aerosol efficiency. It can be used to separate SWARE due to anthropogenic or natural source of aerosols. In Table 2, the instantaneous SW aerosol efficiencies are -45.8 Wm^{-2} τ^{-1}over land and -71.8 Wm^{-2} τ^{-1} over ocean that are both within the range reported by previous regional studies (Christopher et al., 2008; Patadia et al., 2008). Furthermore, diurnal averaged SW efficiencies of aerosols over lands mainly from biomass burning and anthropogenic pollutions are about -26 Wm^{-2} τ^{-1} less negative

when compared with ocean areas with mostly naturally occurring (sea salt) or pollution based (sulfate) aerosols. Based on results for present study, aerosol effect at TOA is cooling the Earth-atmosphere system, whereas surface forcing at the bottom of atmosphere can be further obtained from ground-based measurements or radiative models. Modeling study has shown a diurnal averaged SWARE of -40 Wm^{-2} with an uncertainties of 0 - 4 W/m^{-2} at the surface over Southeast Asia, which is mainly attributable to sulfate, black carbon, and organic carbon (Collins et al., 2002). Larger surface aerosol forcing can be expected in those higher SWARE regions at TOA, however, it will also associated with surface albedo, aerosols and clouds microphysical properties (e.g. phase, size, optical depth) .

3.5 Uncertainty Analysis

There are various sources of uncertainty in data sets. The reported MODIS aerosol uncertainties over land are $\tau = \pm 0.05 \pm 0.15 \times AOD$ (Remer et al., 2005; Levy et al., 2007), while MISR AOD is generally within $\pm 0.20 \times AOD$ of AERONET (Kahn et al., 2005). The recent examination of the MODIS Collection 5 AOD retrieval over global land has been conducted by Hyer et al. (2011) based on comparison with AERONET AODs, which is mostly consistent with previous evaluations. However, they also recommend the greater of 0.08 or $0.02 \pm 0.22 \times \tau$ for Terra MODIS level 2 aerosol data over land, because of complicated boundary conditions and cloud contaminations issues. When satellite products (MODIS and MISR) are compared with surface-based measurements (AERONET), one of the major uncertainty sources comes from the representation of the temporal resolutions from measurement locations relative to the spatial resolution of the satellite products. In this study, AERONET AOD from stations over this region in a period of 30 minutes and satellite retrieved AOD within $0.5° \times 0.5°$ spatial resolutions are

391 collocated in time and space, while 50.6% of MODIS AOD and 43.5% of MISR AOD are found
392 within those uncertainties ranges mentioned above. Much better correlations can be retrieved
393 when higher temporal and spatial resolutions are selected. However, the availability of collocated
394 data points will rapidly decrease with any further increase resolution. Those availabilities are
395 largely affected by issues such as the spatial coverage of sensors aboard satellites and clouds
396 contaminations. It has been described in section 3.3 that algorithm assumptions, calibration
397 methods of satellite retrieved AOD could be the other important source of uncertainties. For
398 example, MODIS AOD retrievals are high-biased compared to AERONET, which have been
399 substantiated by both present and previous and studies (Abdou et al., 2005; Kahn et al., 2005;
400 Zhang and Reid, 2006; Hyer et al., 2011).

401 According to previous studies, the uncertainties in the SWARE value are primarily from five
402 sources including uncertainties in calibrated CERES fluxes (±0.4 Wm^{-2}), conversion between
403 filtered to unfiltered TOA radiances (±0.4 Wm^{-2}), radiance to flux conversion (ADMs) with
404 aerosol effects (±0.4 Wm^{-2}), cloud contaminations (±0.5 Wm^{-2}) and uncertainties in clear sky
405 fluxes estimations (Wielicki et al., 1996; Loeb et al., 2001; Zhang et al., 2005b; Patadia et al.,
406 2008). Since uncertainties in clear sky fluxes are estimated from regression relationship between
407 TOA SW fluxes and MODIS AOD, any uncertainties in fluxes and AOD retrievals will translate
408 to an uncertainty in clear sky fluxes (Christopher, 2011). Patadia et al. (2008) suggested that the
409 uncertainty of clear sky fluxes can be calculated by multiplying the maximum uncertainty in
410 MODIS AOD of 0.05 (Levy et al., 2007) with instantaneous SW efficiency of -45.8 $Wm^{-2}\ \tau^{-1}$
411 over land and -71.8 $Wm^{-2}\ \tau^{-1}$ over ocean, which yields uncertainty in flux of ±1.1 Wm^{-2} over land
412 and ±1.8 Wm^{-2} over ocean (Zhang et al., 2005b). Assuming that all the uncertainties are

uncorrelated, the total uncertainty in SWARE estimations can be estimated using equation (1) (Penner et al., 1994):

$$U_t = \exp[\sum (\log U_i)^2]^{1/2} \text{.....(1)}$$

Where U_i is the uncertainty factor from each individual source of uncertainty and U_t is the total uncertainty factor. Combing all sources of uncertainties based on equation (1), the averaged uncertainties in the instantaneous cloud-free sky SWARE is about 2.1 Wm^{-2} over land and 2.3 Wm^{-2} over ocean. When converting the instantaneous SWARE to a diurnally averaged SWARE value, the uncertainty arises in the scaling factor ($\pm 0.1 Wm^{-2}$). Therefore, the combined uncertainties for present study should be ± 1.2 Wm^{-2} over land and ± 1.3 Wm^{-2} over ocean. Further improvement in retrieval algorithms, instrument calibrations, and multi-angle imaging capabilities are needed to reduce the uncertainties.

4. Summary and conclusions

In this study, we assess the spatial and temporal distributions of the aerosol properties in the Southeast Asia based on multi-sensors (MODIS and MISR) aboard Terra satellite coupled with a quantitative assessment of regional shortwave aerosol radiative effects derived from CERES. Ground-based AERONET data are used to evaluate the performance of MODIS and MISR AODs. The major conclusions are as follows:

1. High aerosol loadings are found over land and ocean close to coastal area in the northern portion of the study region (8°N~25°N), which are due to biomass/coal burning combined with anthropogenic emissions. In the southern region (10°S~8°N), Megacities, e.g. Singapore and Jakarta, are also highly polluted by aerosols from anthropogenic and urban activities. Peak values of AOD (0.42 over land and 0.32 over ocean) occur during winter

436 and spring seasons, which can be transported westward into Indian Ocean by monsoon
437 winds.
438 2. In general, larger areal coverage is an advantage for MODIS. High correlation coefficients
439 of 0.900 and 0.862 are both found in comparisons of AERONET-MODIS and AERONET-
440 MISR, which represent good correlations between satellite and ground-based retrievals
441 over SEA regions although there are over or underestimations in certain AOD ranges that
442 are discussed in this study.
443 3. High AOD values in winter-spring time and low values in summer time can both be seen in
444 MODIS and MISR AOD data. Continuous winter-spring monsoons shift AOD peaks in
445 origin from land to ocean over the period of March to May. High FMFs, (> 70%) ,
446 indicating smaller particle sizes , representing large fractions of biomass burning aerosols
447 and anthropogenic pollutant aerosols are prominent over continental area. Also, high
448 fractions of fine particles over ocean can only be observed in spring months due to
449 atmospheric transport of anthropogenic aerosol particles from land to ocean areas. Higher
450 concentrations of relatively 'dark' aerosols with lower SSA values can be seen in seasonal
451 transition months (e.g. February, March, and September), which indicates an increase of
452 large fractions of strong absorbing aerosols (e.g. biofuel or biomass burning smoke).
453 4. The spatial features of MODIS AODs at 550 nm correspond well with the high SWARE
454 values derived from CERES. The estimated diurnally averaged SWARE in the whole SEA
455 region (5°S~25°N,90°E~150°E) are -6.4±1.2 Wm^{-2} over land area and -5.9±1.3 Wm^{-2} over
456 ocean corresponding to a mean clear-sky total AOD from CERES footprint of 0.27±0.24
457 and 0.12±0.10. This study calculates SWARE by using satellite measurements alone

without any radiative transfer models, therefore is an independent estimation of the aerosol radiative effects at TOA.

To summarize, satellite retrieved aerosol properties are in good agreement with ground-based measurements, though certain amount of errors can still be observed from several sources i.e. complicated low boundary conditions, and cloud contamination. Quality control and assurances process are needed to reduce biases, if those data are further used for radiative effects estimations or data assimilations. Persistent cloud cover in many parts of Southeast Asia is a major problem when working with satellite remote sensing data. Hence data collected from field experiments are critical to acquire aerosols information underneath the cloud layers or close to the surface. The results from this study can be helpful for researchers to assess the locations and periods of field experiments, while they can also be applied to validate model simulations.

Acknowledgements

This research was supported by NASA's Radiation Science, Interdisciplinary Sciences and EOS programs. The authors are thankful to MODIS and MISR aerosol Science team and NASA Langley Research Center Atmospheric Sciences Data Center for providing satellite data. We also thank to the (Project/PI) for (its/theirs) effort in establishing and maintaining AERONET sites used in our investigation.

References

Achard, F. *et al.*, 2002. Determination of Deforestation Rates of the World's Humid Tropical Forests. *Science* 297, 999-1002.

Abdou, W.A. *et al.*, 2005. Comparison of coincident Multiangle Imaging Spectroradiometer and Moderate Resolution Imaging Spectroradiometer aerosol optical depths over land and ocean scenes containing Aerosol Robotic Network sites. *J. Geophys. Res.-Atmos.* 110

Begum, B.A., *et al.*, 2006. Temporal variations and spatial distribution of ambient PM2.2 and PM10 concentrations in Dhaka, Bangladesh. *Sci. Total Environ.* 358, 36-45.

Chi, K.H. *et al.*, 2010. PCDD/F Measurement at a High-Altitude Station in Central Taiwan: Evaluation of Long-Range Transport of PCDD/Fs during the Southeast Asia Biomass Burning Event. *Environ. Sci. & Tech.* 44, 2954-2960.

Chin, M. *et al.*, 2004. Aerosol distribution in the Northern Hemisphere during ACE-Asia: Results from global model, satellite observations, and Sun photometer measurements. *J. Geophys. Res.-Atmos.* 109

Chin, M., *et al.*, 2002. Tropospheric aerosol optical thickness from the GOCART model and comparisons with satellite and Sun photometer measurements. *J. Atmos. Sci.* 59, 461–483.

Collins, W. D., *et al.*, 2002, Simulation of aerosol distributions and radiative forcing for INDOEX: Regional climate impacts, *J. Geophys. Res.* 107, doi:10.1029/2000JD000032, .

Christopher, S.A, 2011. A closer look at the 'clear sky' top of atmosphere shortwave radiative fluxes used for aerosol radiative forcing applications over the global oceans, *Remote Sens. Environ.*, in press.

Christopher, S.A.,Jones, T.A., 2008. Short-wave aerosol radiative efficiency over the global oceans derived from satellite data. *Tellus B* 60, 636-640.

Christopher, S.A., et al., 2006. Satellite-based assessment of top of atmosphere anthropogenic aerosol radiative forcing over cloud-free oceans. *Geophys. Res. Lett.* 33, L15816, doi:10.1029/2005GL025535

Christopher, S.A., Jones, T.A., 2008. Sample bias estimation for cloud-free aerosol effects over global oceans. *IEEE Trans. Geosc. Remote Sens.* 46, 1728-1732.

Chu, D.A. et al., 2005. Evaluation of aerosol properties over ocean from MODIS during ACE-asia. *J. Geophys. Res.-Atmos*. 110, D07308, doi:10.1029/2004JD005208.

Crutzen, P. J., and Andreae M. O., 1990. Biomass burning in the tropics: Impact on atmospheric chemistry and biogeochemical cycles. *Science* 250, 1,669–1,678.

Diner, *et al.*, 1998. Multi-angle imaging spectroradiometer (MISR) instrument description and experiment overview. *IEEE Trans. Geosc. Remote Sens.* 36, 1,072-1,087.

de Meij, A.,Lelieveld, J., 2011. Evaluating aerosol optical properties observed by ground-based and satellite remote sensing over the Mediterranean and the Middle East in 2006. *Atmos. Res.* 99, 415-433.

Edwards, D.P. *et al.*, 2003. Tropospheric ozone over the tropical Atlantic: A satellite perspective. *J. Geophys. Res.-Atmos.* 108,

Gadde, B., et al., 2009. Air pollutant emissions from rice straw open field burning in India, Thailand and the Philippines. *Environ. Pollut.* 157, 1554-1558.

Goldwijk, K., 2001. Estimating global land use change over the past 300 years: The HYDE Database. *Global Biogeochem. Cycles* 15, 417-433.

Heil, A. and Goldammer, J. G., 2001. Smoke-haze pollution: a review of the 1997 episode in Southeast Asia, *Reg. Environ. Change* 2, 24–37.

Holben, B.N. *et al.*, 1998. AERONET--A Federated Instrument Network and Data Archive for Aerosol Characterization. *Remote. Sens. Environ.* 66, 1-16.

Hyer, E. J., Reid, J. S., and Zhang, J., 2011. An over-land aerosol optical depth data set for data assimilation by filtering, correction, and aggregation of MODIS Collection 5 optical depth retrievals. *Atmos. Meas. Tech*., 4, 379-408

Kahn, R.A. *et al.*, 2005. Multiangle Imaging Spectroradiometer (MISR) global aerosol optical depth validation based on 2 years of coincident Aerosol Robotic Network (AERONET) observations. *J. Geophys. Res.-Atmos.* 110

Kahn, R.A. *et al.*, 2007. Satellite-derived aerosol optical depth over dark water from MISR and MODIS: Comparisons with AERONET and implications for climatological studies. *J. Geophys. Res.-Atmos.* 112

Kahn, R.A. *et al.*, 2009. MISR Aerosol Product Attributes and Statistical Comparisons With MODIS. *IEEE Trans. Geosc. Remote Sens.* 47, 4095-4114.

Kaufman, Y., Nakajima T., 1993. Effect of Amazon smoke on cloud microphysics and albedo – Analysis from satellite imagery. *J. Appl. Meteorol.* 32, 729–744.

Kaufman, Y. J., *et al.* , 2002. A satellite view of aerosols in the climate system. *Nature* 419, 215–223.

Kaufman, Y.J. *et al.*, 2005. A critical examination of the residual cloud contamination and diurnal sampling effects on MODIS estimates of aerosol over ocean. *IEEE Trans. Geosc. Remote Sens.* 43, 2886-2897.

Lawrence, M.G.,Lelieveld, J., 2010. Atmospheric pollutant outflow from southern Asia: a review. *Atmos. Chem. Phys.* 10, 11017-11096.

Loeb, N. G., *et al.*, 2001. Determination of unfiltered radiances from the Clouds and the Earth's Radiant Energy System (CERES) instrument. *J. Appl. Meteorol*. 40, 822–835.

Loeb, N.G., *et al.*, 2003. Angular distribution models for top-of-atmosphere radiative flux estimation from the clouds and the earth's radiant energy system instrument on the tropical rainfall measuring mission satellite. part I methodology. *J. Appl. Meteor*. 42, 240–265.

Levy, R.C. *et al.*, 2005. Evaluation of the MODIS aerosol retrievals over ocean and land during CLAMS. *J. Atmos. Sci.* 62, 974-992.

Levy, R.C., *et al.*, 2007. Second-generation operational algorithm: Retrieval of aerosol properties over land from inversion of Moderate Resolution Imaging Spectroradiometer spectral reflectance. *J. Geophys. Res.-Atmos.* 112,

Li, F., Ramanathan, V., 2002. Winter to summer monsoon variation of aerosol optical depth over the tropical Indian Ocean, *J. Geophys. Res. -Atmos.* 107, 4,284.

Liang, Q. *et al.*, 2007. Summertime influence of Asian pollution in the free troposphere over North America. *J. Geophys. Res.-Atmos.* 112

Liu, H.Y. *et al.*, 2003. Transport pathways for Asian pollution outflow over the Pacific: Interannual and seasonal variations. *J. Geophys. Res.-Atmos.* 108

Matsui, H. *et al.*, 2009. Spatial and temporal variations of aerosols around Beijing in summer 2006: Model evaluation and source apportionment. *J. Geophys. Res.-Atmos.* 114

Olivier, J.G.J., Peters, J., 2005. CO2 from non-energy use of fuels: A global, regional and national perspective based on the IPCC Tier 1 approach. *Resour. Conserv. Recycl.* 45, 210-225.

Patadia, F., *et al.*, 2008. A Multisensor satellite-based assessment of biomass burning aerosol radiative impact over Amazonia. *J. Geophys. Res.-Atmos.* 113,

Patadia, F., Christopher S. A., 2010. Top of Atmosphere Smoke Aerosol Radiative forcing over the Amazon from MODIS and CERES using Empirical Angular Models, Part 2 Results. *J. Geophys. Res.-Atmos.* under revision.

Penner, J.E. *et al.*, 1994. Quantifying and minimizing uncertainty of climate forcing by anthropogenic aerosols. *B. Am. Meteorol. Soc. 75,3*, 375-400.

Pochanart, P., *et al.*, 2003. Carbon monoxide, regional-scale transport, and biomass burning in tropical continental Southeast Asia: Observations in rural Thailand. *J. Geophys. Res.-Atmos.* 108,

Prasad, A.K.,Singh, R.P., 2007. Comparison of MISR-MODIS aerosol optical depth over the Indo-Gangetic basin during the winter and summer seasons (2000-2005). *Remote Sens. Environ.* 107, 109-119.

Procopio, A.S. *et al.*, 2004. Multiyear analysis of amazonian biomass burning smoke radiative forcing of climate. *Geophys. Res. Lett.* 31

Reid., J. S., et al., 2005. A review of biomass burning emissions part II: Intensive physical properties of biomass burning particles. *Atmos. Chem. Phys. Disc.* 5, 5,201–5,260.

Reid, J.S. *et al.*, 2009. Global Monitoring and Forecasting of Biomass-Burning Smoke: Description of and Lessons From the Fire Locating and Modeling of Burning Emissions (FLAMBE) Program. *IEEE J. Sel. Top. Appl. Earth Observ. Remote Sens.* 2, 144-162.

Remer, L.A.,Kaufman, Y.J., 2006. Aerosol direct radiative effect at the top of the atmosphere over cloud free ocean derived from four years of MODIS data. *Atmos. Chem. Phys.* 6, 237-253.

Remer, L.A. *et al.*, 2005. The MODIS aerosol algorithm, products, and validation. *J. Atmos. Sci.* 62, 947-973.

Streets, D.G. *et al.*, 2009. Anthropogenic and natural contributions to regional trends in aerosol optical depth, 1980-2006. *J. Geophys. Res.-Atmos.* 114,

Streets, D.G., Yarber, K.F., Woo, J.H.,Carmichael, G.R., 2003. Biomass burning in Asia: Annual and seasonal estimates and atmospheric emissions. *Glob. Biogeochem. Cycle* 17,

Sundarambal, P., Balasubramanian, R., Tkalich, P.,He, J., 2010. Impact of biomass burning on ocean water quality in Southeast Asia through atmospheric deposition: field observations. *Atmos. Chem. Phys.* 10, 11323-11336.

Tang, Y.H. *et al.*, 2003. Influences of biomass burning during the Transport and Chemical Evolution Over the Pacific (TRACE-P) experiment identified by the regional chemical transport model. *J. Geophys. Res.-Atmos.* 108,

Wielicki, B. A., *et al.*, 1996. Clouds and the Earth's Radiant Energy System (CERES): An Earth Observing System Experiment. *Bull. Amer. Meteor. Soc.* 77, 853-868.

Xu, W., *et al.*, 2010. New GOES imager algorithms for cloud and active fire detection and fire radiative power assessment across North, South and Central America. *Remote Sens. Environ.* 114, 1876-1895.

Yu, H. *et al.*, 2006. A review of measurement-based assessments of the aerosol direct radiative effect and forcing. *Atmos. Chem. Phys.* 6, 613-666.

Zhang,J.L., Reid, J.S., 2006. Modis aerosol product analysis for data assimilation: Assessment of over-ocean level 2 aerosol optical thickness products, *J. Geophys. Res.-Atmos.*111, D22207, doi:10.1029/2005JD006898.

Zhang, J.L., Christopher, S.A., Remer, L.A.,Kaufman, Y.J., 2005a. Shortwave aerosol radiative forcing over cloud-free oceans from Terra: 1. Angular models for aerosols. *J. Geophys. Res.-Atmos.* 110,

614 Zhang, J.L., et al., 2005b. Shortwave aerosol radiative forcing over cloud-free oceans from Terra:
615 2. Seasonal and global distributions. *J. Geophys. Res.-Atmos.* 110,
616

617

List of Tables

625 **List of Figures**

626 **Figure 1 MODIS Level1B 550 nm radiances from Terra satellite on Feb. 3rd, 2007. (a) and**
627 **MODIS Level 2 annually averaged aerosol optical depth (AOD) at 550 nm (b) for Southeast**
628 **Asia (10°S~25°N, 90°E~150°E) from the Terra satellite on 2007. The white strips (a) are**
629 **missing data due to orbital gaps. Clouds are shown in white (a) and annual aerosol optical**
630 **depth at 550 nm (b) is shown in various colors ranging from blue to red indicating low to**
631 **high concentrations. (All AERONET sites are located in red points)**

632 **Figure 2 Seasonal variations of Terra-MODIS AOD at 550 nm with NOGAPS winds at**
633 **850hpa averaged over each season and plotted to show transport characteristics (a) winter**
634 **(DJF) (b) spring (MAM) (c) summer (JJA) (d) fall (SON).**

635 **Figure 3 Comparisons of MODIS AOD (a) , MISR AOD (b) and AERONET derived AOD**
636 **at 550 nm wavelength over SEA region during the study period. The solid lines represent**
637 **the slopes of linear regression, the dot lines in (a) represent the retrieval errors of**
638 $\Delta\tau_a = \pm 0.05 \pm 0.15\tau_a$ **and the dot lines in (b) indicate the retrieval errors of**
639 $\Delta\tau_a = \pm 0.2\tau_a$ **.Temporal and spatial standard deviations are shown as the error bars in**
640 **x(AERONET)- and y(MODIS or MISR)-direction, respectively. The colors of polygons**
641 **represent different densities of collocated points.**

642 **Figure 4 The variations of aerosol particle properties over oceans and lands during the**
643 **study period**

644 **Figure 5 SWARE as a function of MODIS AOD for the study area (land and ocean)**

Figure 6 Diurnally average Shortwave Aerosol Radiative Effect spatial distribution for the study area where negative values indicating SW cooling due to aerosols. Aerosol shortwave forcing over land and ocean are calculated respectively, but combined in the same figure.

Table1. Comparisons between AERONET, MODIS and MISR data over Southeast Asia region from December 2006 to November 2007

Site # & name	Lon	Lat	Country /Territory	AERONET(g) vs MODIS(s)				AERONET(g) vs MISR(s)			
				Num	Ground	Satellite	R	Num	Ground	Satellite	R
1.NCU_Taiwan	121.19	24.97	Taiwan	7	0.21±0.13	0.26±0.12	0.83	0	-	-	-
2.Taipei_CWB	121.5	25.03	Taiwan	27	0.40±0.27	0.41±0.31	0.91	2	0.32±0.19	0.28±0.08	1.00
3.EPA-NCU	121.19	24.97	Taiwan	16	0.37±0.25	0.49±0.28	0.94	3	0.48±0.20	0.26±0.08	0.68
4.Lulin	120.87	23.47	Taiwan	17	0.07±0.05	0.17±0.11	0.90	2	0.13±0.08	0.10±0.09	1.00
5.Chen-Kung_Univ	120.22	23	Taiwan	32	0.50±0.33	0.62±0.37	0.90	11	0.41±0.28	0.32±0.14	0.91
6.Bac_Giang	106.23	21.29	Vietnam	24	0.61±0.40	0.78±0.39	0.82	3	0.55±0.33	0.44±0.18	1.00
7.Chiang_Mai_Met_Sta	98.972	18.77	Thailand	14	0.32±0.13	0.24±0.15	0.81	2	0.38±0.07	0.19±0.09	1.00
8.Chiang_Mai	98.987	18.81	Thailand	16	0.72±0.39	0.84±0.49	0.93	3	0.91±0.30	0.49±0.21	0.80
9.Mukdahan	104.68	16.61	Thailand	77	0.44±0.30	0.46±0.34	0.93	10	0.39±0.27	0.31±0.16	0.96
10.Pimai	102.56	15.18	Thailand	93	0.40±0.28	0.45±0.33	0.93	15	0.34±0.17	0.30±0.12	0.96
11.Silpakorn_Univ	100.04	13.82	Thailand	56	0.50±0.20	0.72±0.27	0.91	9	0.51±0.22	0.41±0.16	0.78
12.Bac_Lieu	105.73	9.28	Vietnam	4	0.26±0.17	0.42±0.23	1.00	0	-	-	-
13.Singapore	103.78	1.298	Singapore	3	0.28±0.23	0.76±0.46	0.93	2	0.36±0.32	0.42±0.33	1.00
14.Puspiptek	106.66	-6.356	Indonesia	0	-	-	-	0	-	-	-

Table 2 Shortwave Aerosols Radiative Effects information over Southeast Asia from Terra CERES

	LAND	OCEAN
Clear-sky total AOD	0.27±0.24	0.12±0.10
SW clear sky flux	147.5±16.6 Wm^{-2}	70.1±3.0 Wm^{-2}
SW aerosol sky flux	156.7±21.5 Wm^{-2}	78.4±8.1 Wm^{-2}
Instantaneous SW forcing	-9.2 Wm^{-2}	-8.3 Wm^{-2}
Instantaneous SW efficiency	-45.8 Wm^{-2} τ^{-1}	-71.8 Wm^{-2} τ^{-1}
Diurnal SW forcing	-6.4 Wm^{-2}	-5.9 Wm^{-2}
Diurnal SW forcing efficiency	-20.3 Wm^{-2} τ^{-1}	-34.2 Wm^{-2} τ^{-1}

Figure1. MODIS Level1B radiances from Terra satellite on Feb. 3rd, 2007. (a) and MODIS Level 2 annually averaged aerosol optical depth (AOD) at 550 nm (b) for Southeast Asia (10°S~25°N, 90°E~150°E) from the Terra satellite on 2007. The white strips (a) are missing data due to orbital gaps. Clouds are shown in white (a) and annual aerosol optical depth at 550 nm (b) is shown in various colors ranging from blue to red indicating low to high concentrations. (All AERONET sites are located in red points)

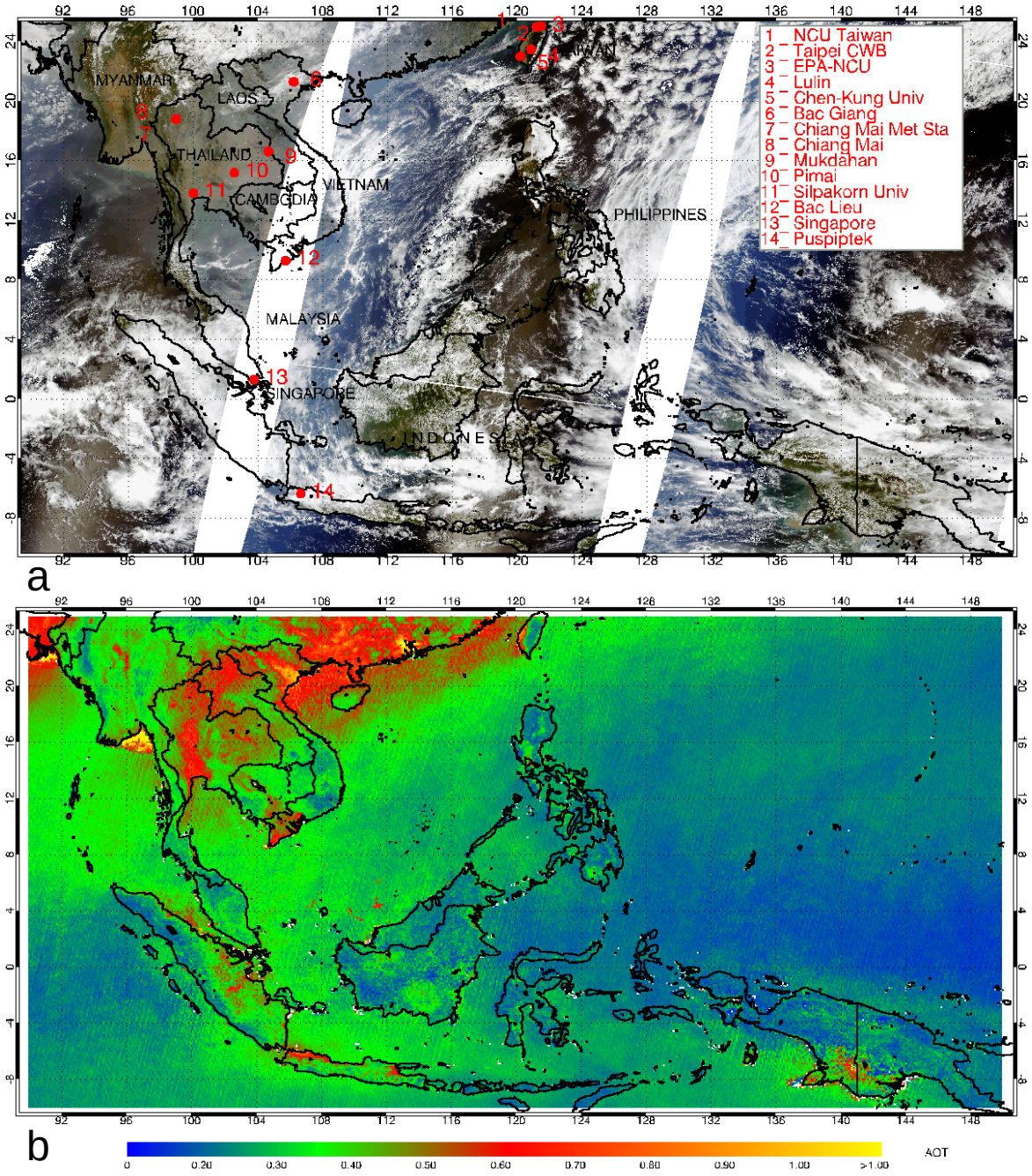

Figure 2 Seasonal variations of Terra-MODIS AOD at 550 nm with NOGAPS winds at 850hpa averaged over each season and plotted to show transport characteristics (a) winter (DJF) (b) spring (MAM) (c) summer (JJA) (d) fall (SON).

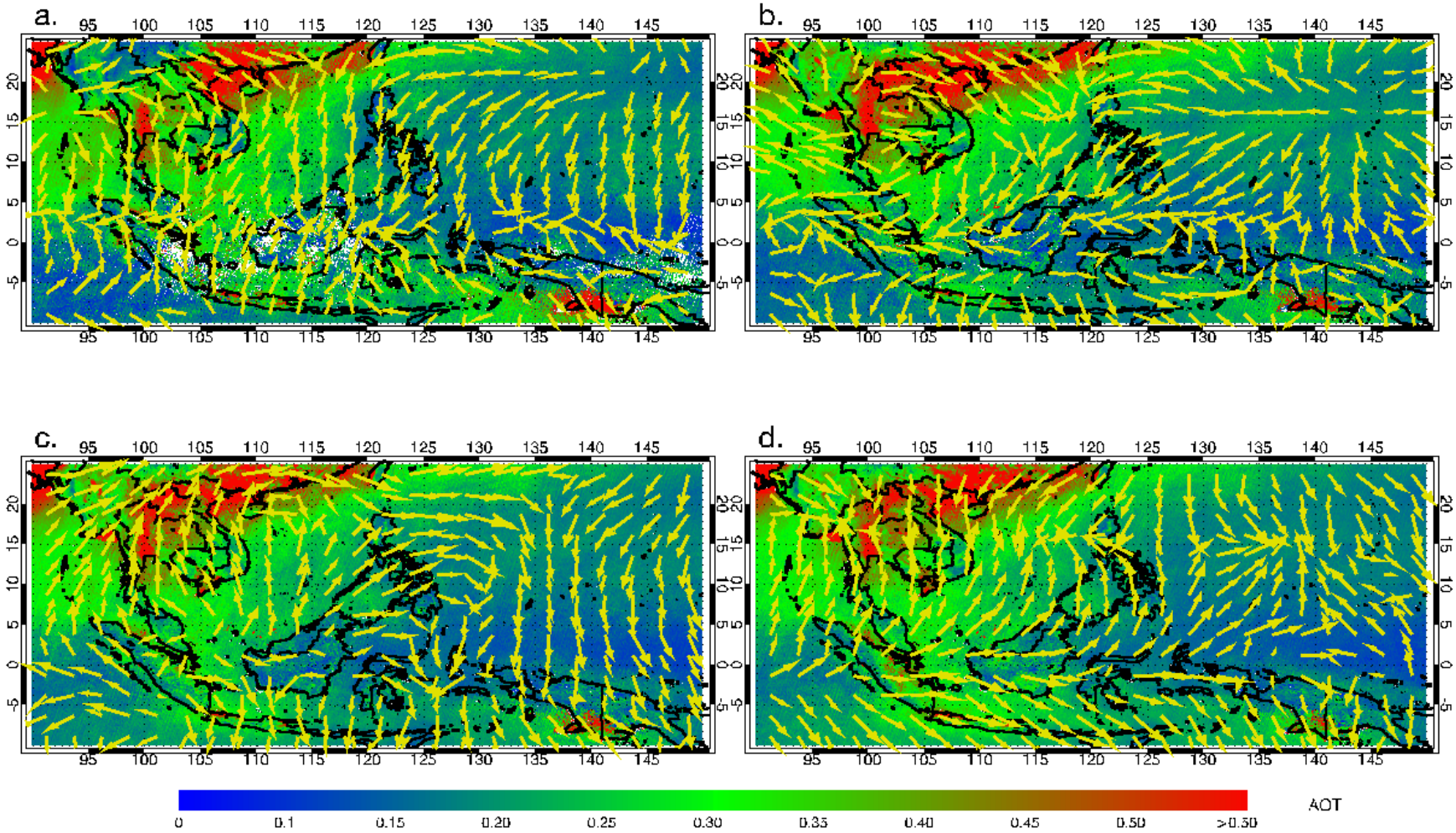

Figure 3 Comparisons of MODIS AOD (a) , MISR AOD (b) and AERONET derived AOD at 550 nm wavelength over Southeast Asia during the study period. The solid lines represent the slopes of linear regression, the dot lines in (a) represent the retrieval errors of $\Delta\tau_a = \pm 0.05 \pm 0.15\tau_a$ and the dot lines in (b) indicate the retrieval errors of $\Delta\tau_a = \pm 0.2\tau_a$. Temporal and spatial standard deviations are shown as the error bars in x (AERONET) - and y (MODIS or MISR)-direction, respectively. The colors of polygons represent different densities of collocated points.

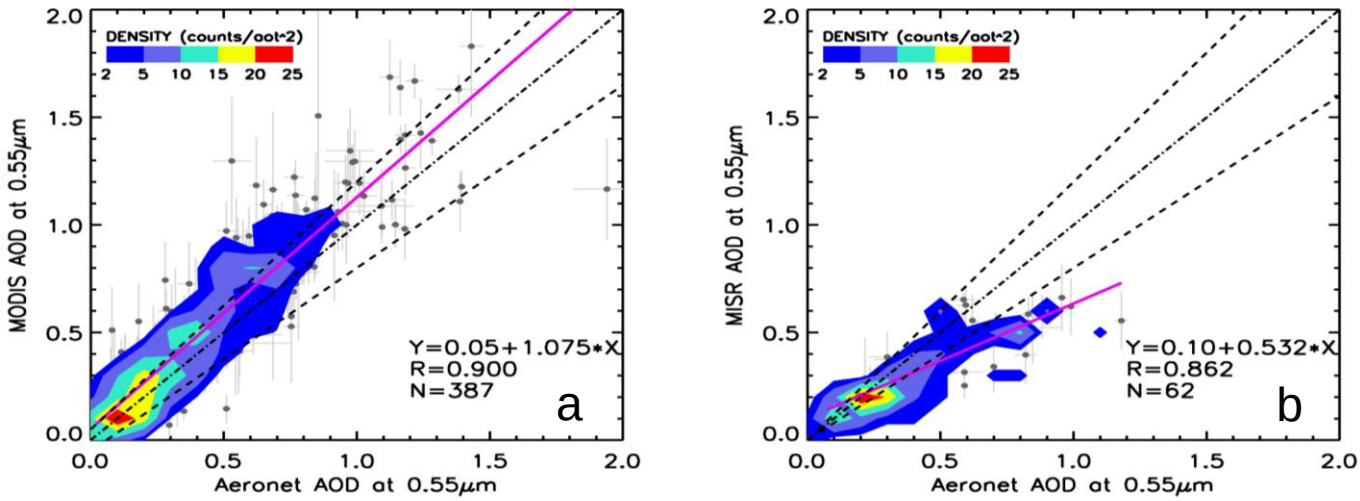

Figure 4 The variations of aerosol particle properties (AOD, FMF, and SSA) over oceans and lands during the study period

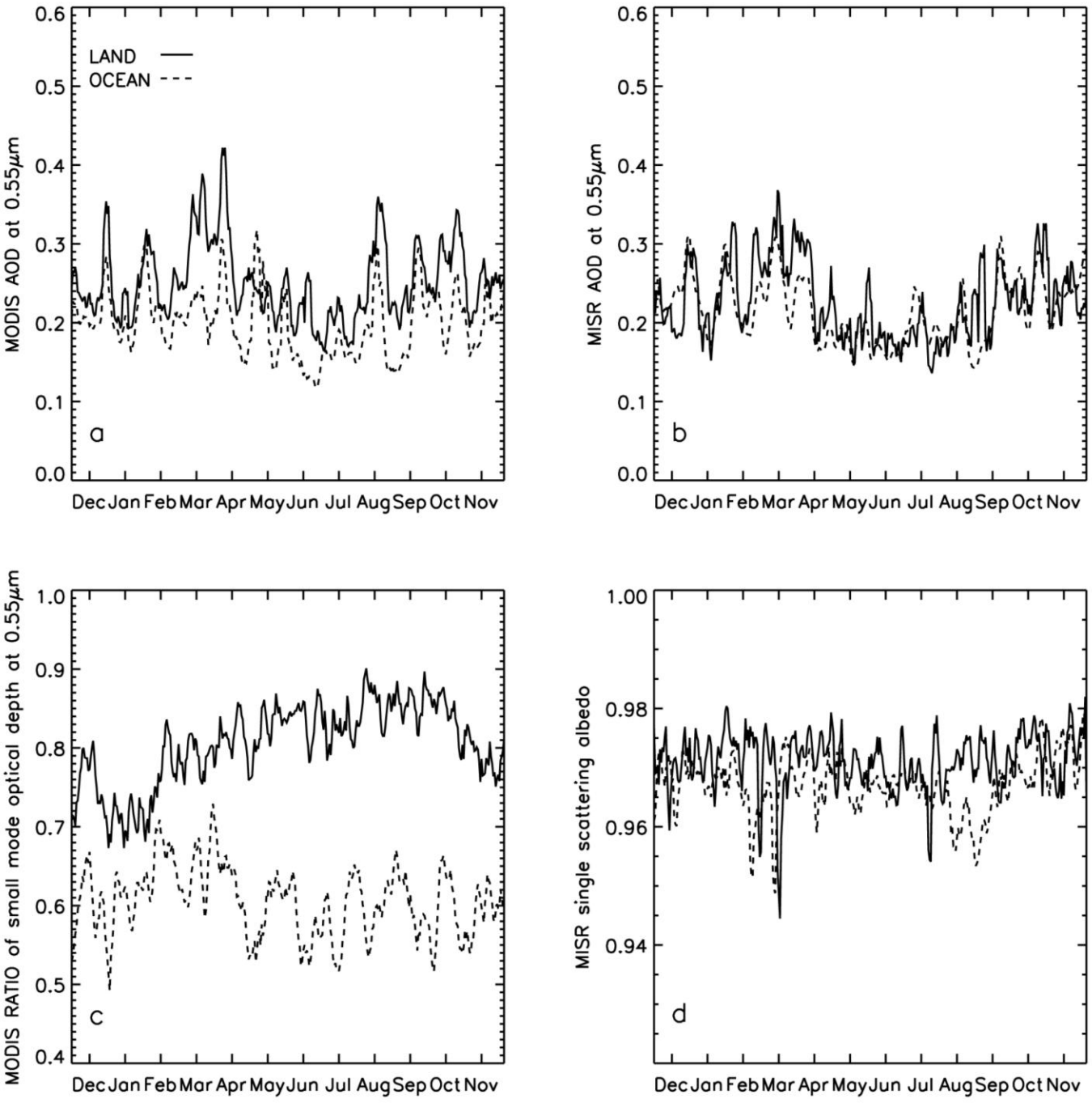

Figure 5 Shortwave Aerosol Radiative Effect as a function of MODIS AOD for the region of interest

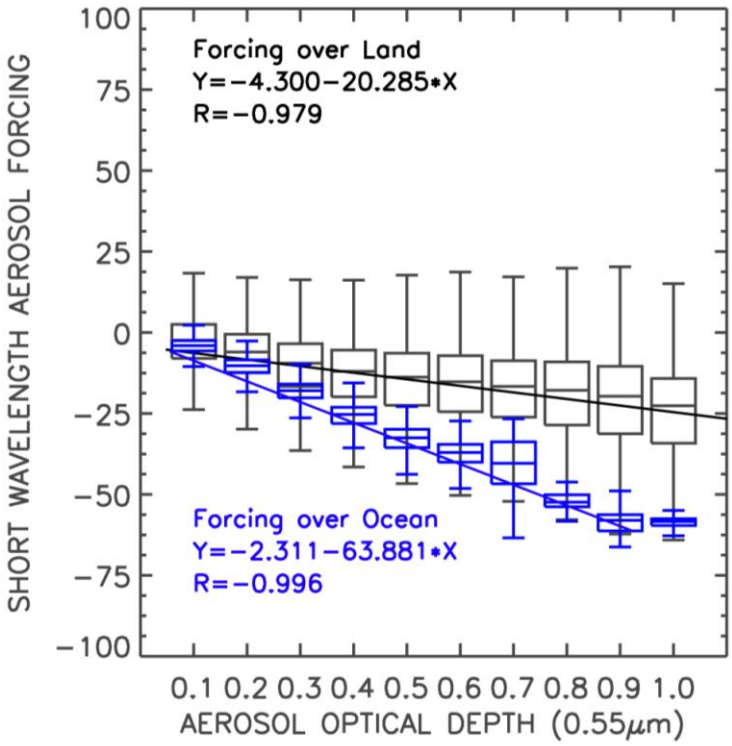

Figure 6 Diurnally average Shortwave Aerosol Radiative Effect spatial distribution for the study area where negative values indicating SW cooling due to aerosols. Aerosol shortwave forcing over land and ocean are calculated respectively, but combined in the same figure.